# Book of Tutorials and Abstracts

European
Microbeam Analysis Society

University of BRISTOL

Mineralogical Society

## EMAS 2018

### 13th EMAS Regional Workshop

## MICROBEAM ANALYSIS IN THE EARTH SCIENCES

4 - 7 September 2018

University of Bristol, Wills Hall, Bristol, Great Britain

Organised in collaboration with:
Mineralogical Society of Great Britain and Ireland
and
University of Bristol

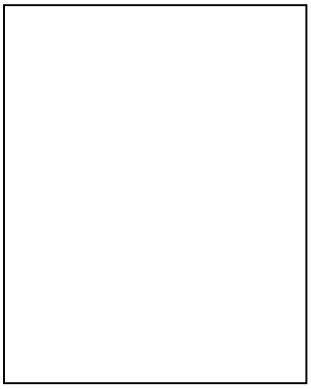

# ANALYSIS OF SULPHUR CONCENTRATIONS AND REDOX STATE IN SILICATE GLASSES

D.J. Smythe, B.J. Wood and W.M. Nash

University of Oxford, Department of Earth Sciences
South Parks Road, Oxford OX1 3AN, Great Britain
e-mail: duane.smythe@earth.ox.ac.uk

*INTRODUCTION*

Sulphur plays an important role in many geological environments. It is a major volatile component in volcanic systems in the form of $SO_2$ and $H_2S$ gases; it is an essential nutrient in sulphate metabolism on the seafloor and it provides sulphide hosts for economically important elements such as Ni, Cu, Pt, and Au. This diverse range of properties is a result of the stabilities of several oxidation states of sulphur in natural environments. The relative stabilities of these different oxidation states control the distribution of sulphur between Earth's various geochemical reservoirs, core, mantle, crust, oceans and atmosphere. They also have profound influence on the distribution of many chalcophile (sulphur-loving) elements between these different reservoirs. For these reasons there have been numerous experimental investigations of the processes that control the incorporation of sulphur in naturally-occurring silicate melts (e.g., [1-5]), however, there are relatively few studies investigating the oxidation sate of sulphur in these systems [6-8].

## *1. THEORETICAL BACKGROUND*

At relatively low oxygen fugacities (i.e., below that of the fayalite-magnetite- quartz (FMQ) buffer) Fincham and Richardson [9] proposed that sulphur dissolves in silicate melts as $S^{2-}$ and that it substitutes for oxygen on the anion sublattice via the reaction:

$$O^{2-} + \frac{1}{2}S_2 = S^{2-} + \frac{1}{2}O_2 \quad (1)$$

In silicate melts the concentrations of $O^{2-}$ are generally two or more orders of magnitude greater than those of $S^{2-}$, even at sulphide saturation. Given this constraint we can take the $O^{2-}$ concentration on the anion sub-lattice to be constant and rearrange the equilibrium constant for reaction (1) to yield the Fincham - Richardson relationship [9]:

$$\ln C_S = \ln[S] + \frac{1}{2}\ln(fO_2/fS_2) \quad (2)$$

In Eq. (2) $C_S$ is the sulphide capacity of the melt (analogous to the equilibrium constant), and [S] is the concentration of sulphur, usually in ppm. Fincham and Richardson [9] experimentally verified the relationship of Eq. (2) by measuring sulphur contents of silicate melts in the system $CaO$-$Al_2O_3$-$SiO_2$ at fixed values of $fS_2$ and $fO_2$. In the geologic literature, most interest has been on the conditions of sulphide saturation and precipitation of sulphides from basaltic and related liquids (e.g., [10, 11]). Nevertheless, O'Neill and Mavrogenes [2] broadened the scope of study by measuring the concentrations of S in 19 melts in the geologically relevant system $CaO$-$MgO$-$Al_2O_3$-$SiO_2$ ± $TiO_2$ ± $FeO$. They showed that, at 1,400 °C and known $fS_2$ and $fO_2$ between -3.36 and 1.59, and -10.92 and -6.78, respectively, all 19 melts obey the Fincham - Richardson relationship.

Under oxidising conditions, Fincham and Richardson [9] observed an increase in log [S] with increasing $fO_2$, indicating that sulphate becomes the dominant species under these conditions. This equilibrium can be expressed through the reaction:

$$\tfrac{1}{2}S_{2\,gas} + \tfrac{3}{2}O_{2\,gas} + O^{2-}_{melt} = SO^{2-}_{4\,melt} \quad (3)$$

As with sulphide, a sulphate capacity parameter ($C_{S^{6+}}$) can be defined and used to express the dependence of concentration on $fO_2$ and $fS_2$. From Eq. (3) we define the equilibrium constant ($K_3$) as,

$$\log K_3 = \log \frac{aSO^{2-}_{4\,melt}}{fS_2^{1/2} \cdot fO_2^{3/2} \cdot aO^{2-}_{melt}} \quad (4)$$

We can then define the sulphate capacity ($C_{S^{6+}}$) by combining $K_4$, $aO^{2-}_{melt}$, and $\gamma SO^{2-}_{4\,melt}$. Rearranging yields;

$$\log [SO^{2-}_{4\,melt}] = \log C_{S^{6+}} + \tfrac{1}{2}\log fS_2 + \tfrac{3}{2}\log fO_2 \quad (5)$$

The transition from sulphide to sulphate with increasing $fO_2$ can readily be understood by combining reactions (1) and (3) as follows:

$$S^{2-}_{melt} + 2O_{2\,gas} = SO^{2-}_{4\,melt} \quad (6)$$

The stoichiometry of this equilibrium, specifically the large number of oxygen atoms required for oxidation, implies that the transition in stability between these species occurs over a narrow $fO_2$ range. This can be shown explicitly if the equilibrium is expressed in terms of the activities or concentrations of its components:

$$\log \frac{[SO^{2-}_4]_{melt}}{[S^{2-}]_{melt}} = \log K' + 2\log fO_2 \quad (7)$$

In Eq. (7) activities have been approximated by concentrations and equilibrium constant $K_7$ replaced by $K'$ (i.e. $K' = K_6 \cdot \gamma S^{2-}_{melt}/\gamma SO^{2-}_{4\,melt}$). The transition from $S^{2-}$ to $SO_4^{2-}$, occurring over the expected narrow $fO_2$ interval, has been observed using the XANES method between FMQ and FMQ+2 by Jugo *et al.* [7] and at FMQ by Klimm *et al.* [12]. Compositional and temperature effects on the transition are unknown. The principal goal of our study was, therefore, to isolate these effects on speciation for a broad range of melt compositions.

## 3. EXPERIMENTAL METHODS

Starting compositions were prepared from powdered oxides and carbonates, which were combined under ethanol into fine homogeneous powders, and decarbonated in air at 1,000 °C. All experiments were conducted in a 1-atmosphere gas-mixing furnace at a constant temperature of 1,300 °C. The oxygen and sulphur fugacities were controlled by continuously flowing appropriate $CO$-$CO_2$-$SO_2$ gas mixtures through the furnace. The gas mixtures required at each $fO_2$ and $fS_2$ were calculated numerically from thermodynamic data for the various C- S and O-bearing species, following the procedure of White *et al.* [13] and flow rates were controlled by standard mass-flow controllers. Based on numerous repeat measurements of $fO_2$ using an ytrria-stabilised zirconia electrolyte we estimate the uncertainty in $fO_2$ as ± 0.1 log units. We chose the highest possible $fS_2$ at each $fO_2$ in order to maximize the sulphur concentration in the melt and obtain XANES spectra with high signal/noise ratios.

## 4. ANALYTICAL METHODS

### 4.1. Sulphur concentration

*4.1.1. EPMA.* The major-element composition of each glass was determined by wavelength-dispersive X-ray spectrometry using a Cameca SX5 electron microprobe at Oxford University. All analyses were conducted with a 15 kV accelerating voltage and a 10 μm, 30 nA electron beam. Standards used for silicate glass analysis were albite (Si, Na), synthetic periclase (Mg), pyrope (Al), sanidine (K), rutile (Ti), Mn metal, Cr metal, fayalite (Fe), and pyrite and barite (S). Peak count times of 20 s where use for Mg, Al, and Si, 30 s for Na, K, Ca, Ti, Cr, Mn, and Fe, and 90 s for S. A natural S-bearing basaltic glass (L17, Edinburgh ion probe facility) containing 48.5 wt% $SiO_2$, 13.2 wt% FeO*, and 1,320 ppm S was used as a secondary standard. The limit of detection for S was ~65 ppm. As the Kα for $S^{6+}$ is approximately 6 eV higher than $S^{2-}$ wave scans were performed on all to find the position of the S peak.

*4.1.2. SIMS.* Sulphur concentrations in all experimental run products were determined by SIMS using a Cameca 1270 mass spectrometer at the Edinburgh University's Materials and Micro Analysis Centre (EMMAC). A glass synthesised at FMQ -1.67 containing 2,121 ppm S was used as the primary standard for all sulphur measurements and the L17 glass was employed as a secondary standard. A caesium primary ion beam of was used, and the instrument calibrated using $^{18}O$ since preliminary analyses revealed $^{18}O$ and $^{32}S$ to have similar ion yields.

### 4.2. Sulphur redox state

*4.2.1. XANES.* X-ray absorption near-edge structure (XANES) spectroscopy has been employed in several studies to measure the relative proportions of $S^{6+}$ and $S^{2-}$ in silicate glasses [8, 14, 15].

The large contrast in electron shielding between the $S^{2-}$ and $S^{6+}$ species gives rise to a difference of ~10 eV in K-edge energy [14] that is easily resolvable using XANES. Previous studies have demonstrated a positive correlation between the energy of the S K-edge and sulphur valence state (e.g., [16-18]), making discrimination between intermediate species (e.g., $S^{-}$, $S^{0}$, $S^{4+}$) also possible. In our study, XANES was used to identify the sulphur species present in synthetic silicate glasses, and to determine their relative abundances by comparing the amplitudes of their characteristic absorption peaks.

Sulphur K-edge XANES spectra were collected on the I18 beamline at the Diamond Light Source synchrotron facility (UK). Spectra were obtained using the Si(111) monochromator, with the instrument in fluorescence mode. The take-off angle was 40°. An energy step-size of 0.25 eV was used across the XANES region, which was broadened to 5 eV at the spectrum extremities to minimise acquisition time while collecting sufficient data for good spectrum normalisation. Multiple spectra were collected for selected glasses to verify instrumental reproducibility.

To minimise potential modification of $S^{6+}/S^{2-}$ during XANES analysis as noted by Wilke *et al.* [19] and Jugo *et al.* [7], a defocussed beam (50 x 50 µm square) was used with the lowest fluence available (~$10^{12}$ photon/sec). The sample, detector, and beam-source were enclosed by a He-filled bag to minimise X-ray absorption and maintain acceptable signal/noise ratios at these low fluences.

Three standards (FeS, S, and $FeSO_4$ powders) were analysed to define the edge positions of the different sulphur species, and to explore the potential for beam-induced damage. The FeS spectrum exhibits a sharp peak at 2,470.4 eV, and a much broader one at 2,478 eV. The 2,470.4 eV peak corresponds to 1*s* to 3*p* and 3*d* transitions [20] and its amplitude has been shown to depend on the cation that $S^{2-}$ is bonded to; transition metal sulphides exhibit a large peak at the energy, and sulphides of Ca and Mg exhibit none at all [17]. The broader feature represents a combination of 1*s* and 3*p* transitions and multiple scattering resonances and is invariably associated with the sulphide ion [20]. Sulphide-saturated basaltic glasses (both natural and synthetic) examined by Jugo *et al.* [7] and Fleet *et al.* [17] exhibit a similar broad feature at this energy, with subtle variations in edge shape that presumably depend on the local bonding environment. Each of the six glasses in this study display this feature when equilibrated under the most reducing conditions, consistent with the dominance of sulphide at low $fO_2$.

The $FeSO_4$ standard exhibits a single sharp peak at 2,482 eV, which is characteristic of excitations from the sulphur 1*s* to the sulphur 3*p* and oxygen 2*p* orbitals of the $SO_4^{2-}$ anion [20]. XANES spectra for sulphate compounds analysed by previous workers have consistently shown this feature (e.g., [7, 18]), and it dominates the spectra of all six melt compositions prepared at the highest $fO_2$, indicating that $S^{6+}$ is the stable sulphur species under the most oxidising conditions. A small peak at this energy is also evident in the spectrum for the FeS standard, suggesting that our FeS powder has undergone some minor oxidation.

Both the high-fluence $FeSO_4$ standard and each of the most oxidised silicate melts exhibit a small peak at 2,478 eV, characteristic of the sulphite ($S^{4+}$) ion [21]. The absence of this peak in the $FeSO_4$ spectrum collected at low-fluence indicates that it is a product of beam damage rather than a feature intrinsic to the standard as shown by Wilke *et al.* [19] and Jugo *et al.* [7].

For each of the six melt compositions studied, the sequence of spectra representing equilibrium under progressively more oxidising conditions display a diminution of the broad feature at 2,476 eV, and its replacement by the sharper peak at 2,482 eV. Each melt composition therefore undergoes the expected transition between sulphide and sulphate stability with increasing $fO_2$. The sequence of spectra for three melt compositions are shown in Fig. 1. Note that the XANES spectra for melts are particularly sensitive to presence of small amounts of sulphate at low $fO_2$ and that this makes the XANES method complementary to SIMS analysis, as discussed below. An increase in spectrum noise with increasing oxidation state is evident, consistent with an observed decrease in S concentration with increasing $fO_2$. From Fig. 1 we can also observe, at fixed $fO_2$ increasing $S^{2-}/S^{6+}$ with increasing FeO content of the silicate melt. This is consistent with the observed increase of sulphide capacity ($C_{S^{2-}}$) with increasing FeO content [2].

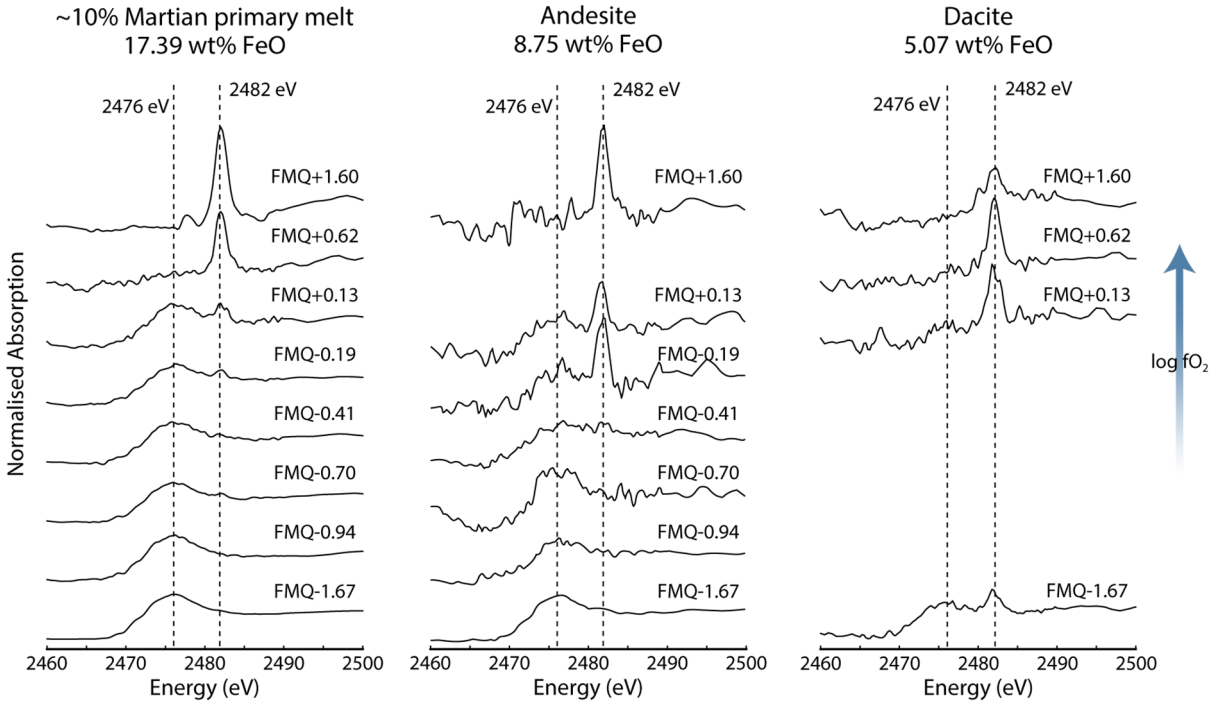


Figure 2. The complete series of XANES spectra for three synthetic glass compositions investigated in this study. Spectra positioned higher in each series represent experiments performed under more oxidising conditions ($fO_2$ conditions labelled relative to FMQ). The change in speciation between sulphide and sulphate is indicated by the progressive diminution of the peak at 2,476 eV and the growth of the peak of 2,482 eV. Signal/noise ratios generally decrease with increasing $fO_2$ due to decreasing S concentration. Horizontally adjacent spectra represent melts at identical $fO_2$ conditions, and comparisons between these – where permitted by an adequate signal/noise ratio – suggests that melts with higher FeO content stabilise sulphate at higher $fO_2$.

The fractions of S as $S^{6+}$ in our glasses ($S^{6+}/\Sigma S$) were calculated by linear combination fitting of spectra representing fully reduced and fully oxidised glasses using the software Athena [22]. We also took account of the observation that $S^{6+}$ absorbs more strongly than $S^{2-}$ [7, 23]. The latter effect is approximately a factor of 3 [23] and we assumed exactly 3 because this gives reasonable agreement with the calibration curve of Jugo *et al.* [7].

The calculated fractions of $S^{6+}$ for each melt at the different $fO_2$ conditions are shown plotted against ΔFMQ in Fig. 2. Also shown in Fig. 2 are the theoretical oxygen fugacity curves for addition of $2O_2$ to $S^{2-}$ (as in reaction 7) assuming that activity coefficients for $S^{2-}$ and $SO_4^{2-}$ are constant and unaffected by $fO_2$. The curves were fitted to the results for a FeO rich basalt (JFR) and andesitic (AND) compositions.

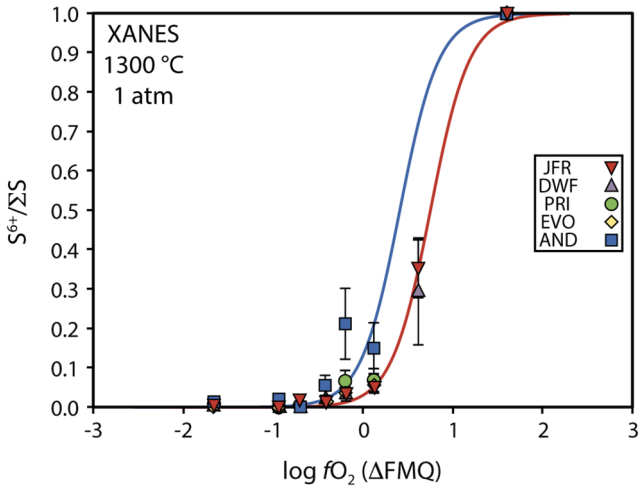


Figure 2. Fraction of S as $S^{6+}$ determined by XANES spectroscopy plotted against log $fO_2$ of equilibration relative to the FMQ buffer. Experiments with excessively noisy spectra yielding errors greater than 0.15 $S^{6+}/\Sigma S$ have been omitted from the figure. The smooth curves are best fits to the JFR (red), and AND (blue) assuming a sulphide-oxidation equilibrium of the form given in Eq. 8. Errors in sulphate mole fraction have been calculated individually based on the variation in permissible end-member weightings during LCF. Errors in $fO_2$ are 0.1 log units.

*4.2.2. From concentration.* Total sulphur concentrations measured by SIMS are plotted on a log-log scale against $fS_2/fO_2$ ratio in Fig. 3. The proportionality relation arising from the sulphide dissolution reaction (Eq. 3) should emerge as a straight line of gradient 1/2 in the data. Points lying above the line reflect increasing $S^{6+}$ in the melt. As observed in earlier studies at 1 atm [9, 10] the S-concentration reaches a minimum on approaching the $S^{2-}$ to $S^{6+}$ transition.

As can be seen from Fig. 3, both the DAC and JFR compositions fit the theoretical log [S] versus log ($fS_2/fO_2$) slope corresponding to dominance of $S^{2-}$ at all $fO_2$'s below FMQ. The same applies for all six melt compositions studied including DAC despite the presence of $S^{6+}$ in the XANES spectrum of this sample, which we attribute to beam damage. Positive deviations from the

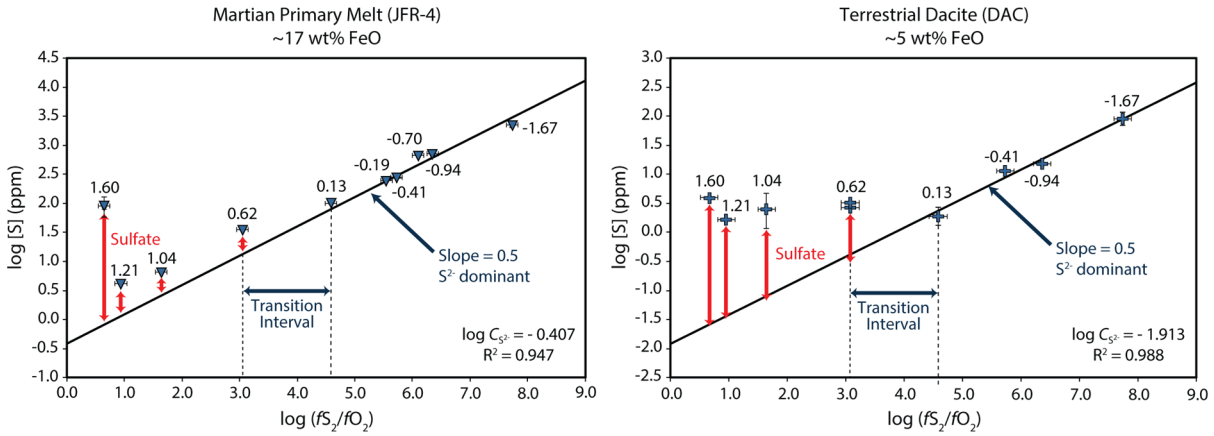


Figure 3. The logarithm of total sulphur concentration (determined by SIMS) plotted against the logarithm of the $fS_2/fO_2$ ratio, for the JFR and terrestrial DAC compositions. The $fO_2$ conditions of each experiment are individually labelled in log units relative to the FMQ buffer. Experiments lying further towards the left represent more oxidising conditions. The black lines are weighted linear best-fits to experiments equilibrated at FMQ+0.13 and below, with gradients fixed at 1/2, thereby representing the sulphide-dissolution equilibrium (Eqs. 1-3). Melts with constant sulphide capacity are expected to lie along this slope, and positive deviations are interpreted as indicative of sulphate. Values for log $C_{S^{2-}}$ correspond to the y-intercept (Eq. 3).

predicted "sulphide slope" occur for every melt composition, confirming the presence of an oxidized sulphur species, which our spectroscopic measurements indicate to be $S^{6+}$. The size of these deviations from the "sulphide slope" and the implied quantities of $S^{6+}$, are indicated in Fig. 3 by the red arrows. The SIMS data show that the transition from $S^{6+}/\Sigma S$ of <0.05 to $S^{6+}/\Sigma S$ of >0.95 lies between FMQ+0.13 and FMQ+0.62 for all six melts. Note, however, that the method is insensitive to small amounts of $S^{6+}$ because of the requirement to fit the ½ slope through the data points under the most reducing conditions. This constraint makes the first ~30 % of $S^{6+}$ difficult to quantify. The SIMS method is therefore most accurate under oxidizing conditions where the deviations from the ½ slope of Fig. 3 are large.

Figure 4 shows measurements of sulphur speciation as a function of $fO_2$ as determined by the sulphur concentration of our samples. We excluded results where the propagated uncertainty exceeded 15 % of the $S^{6+}/\Sigma S$ value. As can be seen in Fig. 4 there is very good agreement between the two methods and a continuous line of crossover from $S^{2-}$ to $S^{6+}$ can readily be constructed. The spread as a function of melt composition is small and behaviour of our dacite composition appears to be consistent with that of the other melts.

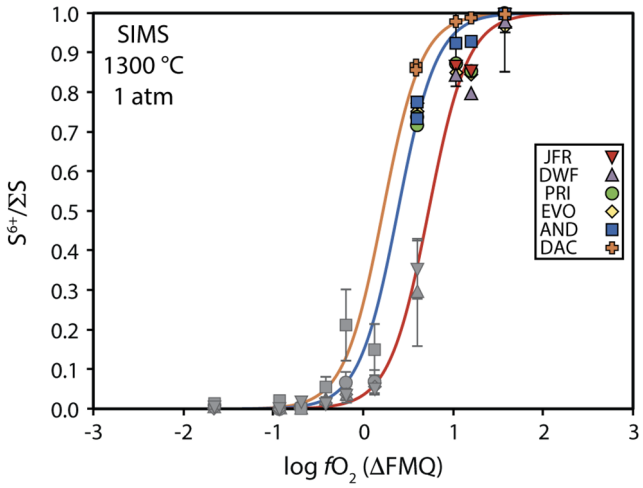


Figure 5. Fraction of S as $S^{6+}$ derived from SIMS analyses plotted against $fO_2$. Sulphate mole fractions were determined by subtracting modelled sulphide concentrations from the SIMS analyses of total sulphur (i.e., from the deviations in log [S] from the "sulphide-slopes" in Fig. 4). $S^{6+}/\Sigma S$ of grey symbols were determined by XANES spectroscopy (shown in Fig. 2). The smooth curves are weighted best fits to the JFR (red), AND (blue), and DAC (orange) assuming a sulphide-oxidation equilibrium of the form given in Eq. 8. In contrast to the tentative prediction made by XANES, the sulphide-sulphate transformation for the DAC composition occurs here at $fO_2$ conditions much closer to those of the other 5 melts.

## 5. *CONCLUSIONS*

Based on the SIMS analyses we are confident that the conditions of crossover from $S^{2-}$ to $S^{6+}$ are accurately represented by the XANES spectra for 5 of the 6 melts studied. The exception is the dacite melt which appears to contain significant sulphate even at the lowest $fO_2$ employed (Fig. 1). This result is inconsistent with SIMS results for the dacite (discussed below) which indicate that $S^{2-}$ is dominant at all oxygen fugacities below FMQ+0.13 (Fig. 3). Although we do not have an unequivocal explanation for the aberrant result, we suspect that it arises from a combination of photo-oxidation of the glass during collection of the spectrum and the low concentrations of sulphur in these samples resulting in a low signal to noise ratio. This makes the SIMS method complementary to the XANES approach since the latter enables detection of small amounts of $S^{6+}$ but decreases in accuracy at high $fO_2$ because of the declining sulphur concentrations (Fig. 1).

## 6. *REFERENCES*

[ 1] Shima H and Naldrett A J 1975 Solubility of sulphur in an ultramafic melt and the relevance of the system Fe-S-O. *Econ. Geol.* **70** 960-967

[ 2] O'Neill H St C and Mavrogenes J A 2002 The sulphide capacity and the sulphur content at sulphide saturation of silicate melts at 1400°C and 1 bar. *J. Petrology* **43** 1049-1087

[ 3] Li C and Ripley E M 2005 Empirical equations to predict the sulphur content of mafic magmas at sulphide saturation and applications to magmatic sulphide deposits. *Mineralium Deposita* **40** 218-230
[ 4] Liu Y, Samaha N-T and Baker D R 2007 Sulphur concentration at sulphide saturation (SCSS) in magmatic silicate melts. *Geochim. Cosmochim. Acta* **71** 1783-1799
[ 5] Smythe D J, Wood B J and Kiseeva E 2017 The S content of silicate melts at sulphide saturation: new experiments and a model incorporating the effects of sulphide composition. *Amer. Mineralogist* **102** 795-803
[ 6] Carroll M R and Rutherford M J 1988 Sulphur speciation in hydrous experimental glasses of varying oxidation states: Results from measured wavelength shifts of sulphur X-rays. *Amer. Mineralogist* **73** 845-849
[ 7] Jugo P J, Wilke M and Botcharnikov R E 2010 Sulphur K-edge XANES analysis of natural and synthetic basaltic glasses: Implications for S speciation and S content as function of oxygen fugacity. *Geochim. Cosmochim. Acta* **74** 5926-5938
[ 8] Botcharnikov R E, Linnen R L, Wilke M, Holtz F, Jugo P J and Berndt J 2011 High gold concentrations in sulphide-bearing magma under oxidizing conditions. *Nature Geosci.* **4** 112-115
[ 9] Fincham C J B and Richardson F D 1954 The behaviour of sulphur in silicate and aluminate melts. *Proc. Royal Soc. A: Math., Phys. Engng. Sci.* **223** 40-62
[10] Katsura T and Nagashima S 1974 Solubility of sulphur in some magmas at 1 atmosphere. Geochim. Cosmochim. Acta 38 517-531
[11] Wallace P J and Carmichael I S E 1992 Sulphur in basaltic magmas. *Geochim. Cosmochim. Acta* **56** 1863-1874
[12] Klimm K, Kohn S C, O'Dell L A, Botcharnikov R E and Smith M E 2012 The dissolution mechanism of sulphur in hydrous silicate melts. II: solubility and speciation of sulphur in hydrous silicate melts as a function of $fO_2$. *Chem. Geol.* **322-323** 250-267
[13] White W B, Johnson S M and Dantzig G B 1958 Chemical equilibrium in complex mixtures. *J. Chem. Phys.* **28** 751-755
[14] Métrich N, Berry A J, O'Neill H St C and Susini J 2009 The oxidation state of sulphur in synthetic and natural glasses determined by X-ray absorption spectroscopy. *Geochim. Cosmchim. Acta* **73** 2382-2399
[15] Brounce M, Stolper E and Eiler J 2017 Redox variations in Mauna Kea lavas, the oxygen fugacity of the Hawaiian plume, and the role of volcanic gases in Earth's oxygenation. *Proc. Natl. Acad. Sci.* USA **114** 8997-9002
[16] Paris E, Giuli G and Carroll M R 2001 The valence and speciation of sulphur in glasses by X-ray absorption spectroscopy. *Can. Mineralogist* **39** 331-339
[17] Fleet M E, Liu X, Harmer S L and King P L 2005 Sulphur K-edge XANES spectroscopy: chemical state and content of sulphur in silicate glasses. *Can. Mineralogist* **43** 1605-1618
[18] Almkvist G, Boye K and Persson I 2010 K-edge XANES analysis of sulphur compounds: an investigation of the relative intensities using internal calibration. *J. Synchrotron Rad.* **17** 683-688

[19] Wilke M, Jugo P J, Klimm K, Susini J, Botcharnikov R, Kohn S C and Janousch M 2008 The origin of $S^{4+}$ detected in silicate glasses by XANES. *Amer. Mineralogist* **93** 235-240

[20] Wilke M, Klimm K and Kohn S C 2011 Spectroscopic studies on sulphur speciation in synthetic and natural glasses. *Rev. Mineral. Geochem.* **73** 41-78

[21] Métrich N , Bonnin-Mosbah M, Susini J, Menez B and Galoisy L 2002 Presence of sulphite ($S^{IV}$) in arc magmas: Implications for volcanic sulphur emissions. *Geophys. Res. Lett.* **29**(11) 33

[22] Ravel B and Newville M 2005 ATHENA, ARTEMIS, HEPHAESTUS: data analysis for X-ray absorption spectroscopy using IFEFFIT. *J. Synchrotron Rad.* **12** 537-541

[23] Jalilehvand F 2006 Sulphur: not a "silent" element any more. *Chem. Soc. Rev.* **35** 1256-1268